Microchemical Journal 170 (2021) 106693

Contents lists available at ScienceDirect

Microchemical Journal

journal homepage: www.elsevier.com/locate/microc

New models involving quantum chemical parameters for assessing the chromatographic retention process

F.J. Pereira [a], R. López [b], A. Rodríguez-Cordero [a], L.C. Robles [a], D. Suárez [c], A.J. Aller [a,*]

[a] Department of Applied Chemistry and Physics, Area of Analytical Chemistry, Faculty of Biological and Environmental Sciences, Campus de Vegazana, s/n, University of León, E-24071 León, Spain
[b] Department of Applied Chemistry and Physics, Area of Physical Chemistry, Faculty of Biological and Environmental Sciences, Campus de Vegazana, s/n, University of León, E-24071 León, Spain
[c] Department of Physical and Analytical Chemistry, Area of Physical Chemistry, University of Oviedo, Julián Clavería 8, 33006 Oviedo, Spain

ARTICLE INFO

Keywords:
RP-HPLC
Structure-retention relationship
Drugs
Mathematical modelling
Gumbel distribution
Quantum parameters

ABSTRACT

Knowledge about the theoretical relationship between the analyte properties and the critical chromatographic parameters is mandatory for a better interpretation of the separation mechanism and a more leisurely development of quantitative studies. In a preliminary stage of this work, we introduce the Gumbel distribution, the extreme value distribution type-I widely used in other fields, as a novel tool for modelling the chromatographic peak shape. Further, we develop mathematical models to evaluate the effect of the experimental variables and various quantum parameters on the chromatographic indices, such as the retention time, capacity factor, asymmetry factor, tailing factor and number of theoretical plates. Finally, we propose a mechanistic behaviour for the chromatographic separation process based on the structure-retention relationship of fifteen selected drugs involving several molecular quantum parameters.

1. Introduction

High-Performance Liquid Chromatography (HPLC) is today the analytical technique of choice for separating many analytes. A better conceptualisation of the chromatographic separation process could achieve if theoretical models are developed, allowing more accurate generalisations and predictive powers. In HPLC, it is usual to assume symmetric (Gaussian) peaks for theoretical, quantitative studies. However, more frequent than usual, the chromatographic responses show asymmetric peaks, generating bias in their location and quantification [1]. Further, variations of the peak width, w, and the back, $A_{0.1}$, and the front, $B_{0.1}$, regions of the chromatographic peak, modify the column resolution and the number of theoretical plates. Hence, using simple mathematical models, incorporating parameters directly derived from the experimental asymmetric peaks, is necessary for an accurate theoretical quantification [2]. In this way, mathematical modelling of the peak shape facilitates the interpretation of the analyte behaviour on the column and evaluates the effect of the chromatographic retention parameters. Many theoretical and empirical models, mainly based on exponential and Gaussian functions [2–11], have been widely assayed to fit the peak shape. Other models include Lorentzian, hyperbolic, and logistic functions, together with different experimental chromatographic parameters [2,9,11,12].

Notwithstanding, the chromatographic retention process depends strongly on the chemical nature of the stationary and mobile phases, although also modulated by the selected values of the experimental variables. However, the structure-dependent properties of the analytes also contribute prominently to the possible mechanistic interpretation [13]. In this way, several works have been focussed on the theoretical evaluation of the separation process, relating the capacity factor with different experimental and structural parameters, such as mobile phase composition, polarity, and acid-base characteristics [14–18]. Nonetheless, the involvement of the quantum chemical parameters on the retention mechanism needs additional clarification for a better interpretation of the separation process. Hence, the combination of macro and micro-approaches is very appropriate to improve the understanding of the chromatographic separation process.

In this work, we successfully use a statistical approach, the Gumbel distribution, an extreme value distribution type-I [19,20], widely used in other fields but incorporated in this work as a novelty in chromatography to model the chromatographic peak shape. Among the three extreme value models, we select the Gumbel-type distribution because

* Corresponding author.
E-mail address: aj.aller@unileon.es (A.J. Aller).

https://doi.org/10.1016/j.microc.2021.106693
Received 15 February 2021; Received in revised form 18 July 2021; Accepted 26 July 2021
Available online 28 July 2021

both the domain of this function is the set of all real numbers, and a rigid body of mathematical theory is behind it. For comparison purposes and to achieve an accurate evaluation of the behaviour of this function, we use as reference two well-established models in chromatography, the empirical Bi-Gaussian [7] and the Exponentially Modified Gaussian (EMG) [12,21] functions. The last one is generally seen as the best model to describe the chromatographic peak shape [22,23]. On the other hand, we use correlation analysis to establish sound theoretical relationships between some chromatographic variables, such as retention time, capacity factor, tailing factor, asymmetry factor and number of theoretical plates, with several quantum chemical parameters. We select the energy bandgap (GAP or ΔE), dipole moment (μ), polarizability (α), solvent accessible surface (SAS), polar molecular surface (SEP), %SEP/SAS ratio, and two electrostatic potentials for heteroatoms (VPOT_X) and hydrogen atoms (VPOT_H) as the most representative quantum chemical parameters potentially involved in the chemical interactions with other molecules in solution and solid phase. To carry out the study, we routinely use the methanol-based mobile phase to assay a first group of drugs: paracetamol, caffeine, tramadol, salicylic acid, phenylephrine, propranolol hydrochloride, acebutolol hydrochloride, nadolol and atenolol, some of them already successfully evaluated by us [24]. However, we try to extend the applicability of the structure-retention relationship to other analytes and chromatographic conditions. In this way, we include a second group of analytes with very different chemical and structural properties, such as cetirizine hydrochloride, estradiol, estrone, diethylstilbestrol, ibuprofen, and progesterone, using acetonitrile as a less polar mobile phase. We choose the drugs according to their applicability and commercial availability and some variability in the molecular mass, structural geometry, acidic character, molecular size, and size of the conjugated system. As a result, we expect to understand better the structure-retention relationship of the analytes, which allows us to anticipate suitable potential chromatographic uses and clear elucidation of their chemical behaviour under different situations.

2. Experimental

2.1. Instrumentation and statistical software

We used an HPLC Alliance, Waters 2690 Separations Module (Waters Corporation, Milford, Massachusetts, USA), including controller, autosampler and thermostatic column oven. Chromatographic separation was on a SunFire^{TM} C_{18} column, 4.6 × 250 mm, 5 μm from Waters, including a Rheodyne injector with a 20 μL fixed loop. A Waters 996 Photodiode Array Detector, with variable wavelength (210–400 nm) programmable UV detector. For data analysis, we use Empower software (Scarborough, Western Australia). Absorbance measurements were recorded on a Thermo Spectronic Helios Alpha 9423 UVA 1002E UV–Vis Double beam Spectrophotometer (Thermo Fisher Scientific Inc., Waltham, MA, USA), combining a deuterium-discharge lamp for the ultraviolet (UV) wavelength range and a tungsten lamp for the visible and short wave near-infrared (SWNIR) wavelength range. We developed UV–Vis absorption spectra of the analytes in aqueous solutions at pH 5.0, selecting the 210 nm line as the optimum analytical wavelength for absorbance detection.

The chromatograms and UV–Vis spectra were processed using the Microcall Origin Software 9.0. A Bransonic sonicator, model B-5 (Soest, The Netherlands), was used for degasification of the sample solutions. To measure the acidity of the aqueous phase, we used a pH meter (Crison model Digit 505) when necessary and a Mettler AE 240 semi-micro analytical balance (sensitivity = 0.01 mg) for weighing the solid chemicals when necessary.

To fit the effect of the experimental variables and the molecular quantum parameters, we used the R statistical software packages R 3.6.2 and R 4.0.2 [25] and Excell 2019. Alternatively, to develop other statistical calculations, we used Microcall Origin Software 9.0, SPSS v.26, while the chromatographic peaks were digitised using GetData Graph Digitizer 2.26.

2.2. Computational methods

The quantum chemical parameters studied were the HOMO-LUMO energy gap (GAP or ΔE), dipole moment (μ), polarizability (α), solvent accessible surface (SAS), and polar molecular surface (SEP). To assess the role of the electrostatic potential as a possible exciting index in the hydrogen bond formation between the drug and the mobile phase, as suggested by Galabov et al. [26], the electrostatic potential without nuclei contributions at the Lewis base sites: 'O', 'OH', 'OS' and 'N' (VPOT_X), and the Lewis acid sites 'H-O' and 'H-N' (VPOT_H) were also computed.

The OpenBabel [27] suite generated initial geometries, followed by an automatic conformational search using the multi conformer generator MS-DOCK [28]. For each drug, up to 50 different conformers were generated, in turn, optimised and scored using the MMFF4 force field as implemented in OpenBabel. Afterwards, we optimised the 10 more stable conformers by quantum chemical calculations at the B3LYP/6–31 + G* level of theory, which combines the popular density functional B3LYP method [29,30] with the Pople's double-ζ basis [31–33]. The SMD solvation model [34] was also employed, selecting water as the continuum solvent. In addition, the third-generation dispersion (D3) correction using the Becke-Johnson damping function was included [35]. We refined the geometry of the most stable conformer at the B3LYP-D3/aug-cc-pVDZ SMD level (using the Dunning's double-ζ basis set [36,37]) followed by analytical Hessian calculations that confirmed the signature of the critical points as energy minima. We carried out all the B3LYP-D3 calculations with the Gaussian 16 package [38].

Hait and Head-Gordon [39,40] have benchmarked many DFT methods for predicting dipole moments and polarizabilities of organic molecules, finding that the double-hybrid density functional PWPB95 [41,42] performs very well. Thus, the quantum chemical parameters of each drug derived from single-point PWPB95/aug-cc-pVTZ calculations on the B3LYP-D3/aug-cc-pVDZ SMD geometry of their most stable conformer using the *Orca* package [43,44]. We considered the same geometries to obtain the solvent-accessible surface areas (SASs) using the *Chimera* program [45,46] with default atomic radii and a solvent probe radius of 1.4 Å.

2.3. Chemicals and reagents

All chemicals and solvents used were HPLC grade. Methanol (MeOH) (Purity > 99%) was from Labscan Limited, Dublin, Ireland, while we prepared phosphate buffers weighing and pipetting the appropriate amount of orthophosphoric acid (H_3PO_4) (1.71 Kg/L, 85%), dipotassium hydrogen phosphate (K_2HPO_4) or potassium dihydrogen phosphate (KH_2PO_4) (Panreac, Barcelona, Spain). We degassed buffer solutions using an ultra sonicator and adjusted the pH of the resulting solutions to the desired value after the addition of methanol.

The analytes were of the highest purity. The analytes were from Sigma-Aldrich (St. Louis, Missouri, USA): paracetamol, caffeine, tramadol, salicylic acid, phenylephrine, acebutolol hydrochloride, nadolol, atenolol, and cetirizine hydrochloride), Roig Farma SA (Terrassa, Barcelona, Spain): propranolol hydrochloride, estrone, estradiol 17α, diethylstilbestrol, and ibuprofen, Acopharm (Madrid, Spain): phenylephrine chlorhydrate, and Fagron (Rótherdam, Netherlands): progesterone. Other general reagents were from Merck (Darmstadt, Germany). We prepared standard stock solutions by weighing accurately 25 mg of the pure drugs, dissolved in 10 mL mobile phase, transferred into a 25 mL volumetric flask and made up to the mark. The solution was made up to the mark with the mobile phase, filtering through a 0.45 μm membrane filter. We used Milli-Q water (18 MΩcm) and sonication for 15 mi to prepare all solutions.

2.4. Chromatographic conditions

We carried out a systematic and detailed study of the effect of the experimental chromatographic variables: mobile phase composition (% MeOH/%Phosphate solution ratio in the range 20/80 v/v – 60/40 v/v), pH (4.0–8.0), phosphate concentration (0.003–0.06 M), and flow rate (FR) (0.4–1.2 mL/min). For simplification purposes, we select as reference experimental conditions the following: mobile phase with a % MeOH/%Phosphate solution ratio of 40/60 v/v, pH 4.5, phosphate concentration 0.006 M, and flow rate (FR) 1 mL/min. The acetonitrile-based mobile phase composition was similar to replacing methanol with acetonitrile (40%Acetonitrile/60%Phosphate solution ratio v/v), using the other variables in the same way.

The chromatographic parameters include an isocratic operation, room temperature, detection at 210 nm, injection volume of 20 μL, and the maximum run time of 45 min working with methanol and 120 min with acetonitrile. The addition of phosphate allows us to control the potential effect of the ionic strength of the mobile phase. In this work, we used adjusted retention times for theoretical calculations.

To adopt the quality by design (QbD) guidelines from the International Conference on Harmonization (ICH) [47], suitability tests to ascertain the effectiveness of the chromatographic procedures were carried out on freshly prepared stock standard solutions to verify the validation of the chromatographic system. The experimental data used along the work were the average of at least three measurements.

3. Results and discussion

To establish an initial experimental chromatographic reference, we include two chromatograms (Fig. SI-1) related to separating both groups of analytes using the mobile phases based on methanol and acetonitrile.

3.1. Preliminary fits

Firstly, we made tentatively the fitting of the peak shape using seven models (Table SI-1). Three of the models, the Chesler-Cram Peak Function (CCE, defined by eight variables), the Edgeworth-Cramer Peak Function (ECS, defined by five variables) and the continuous probability distribution of a random variable whose logarithm is normally distributed (LogNormal, defined by three variables), provided the worst fits (Fig. SI-2). The Gram-Charlier Peak Function (GCAS, defined by five variables) was very suitable in the fit, but ECS and CCE use complex (polynomial) equations. The above four models incorporate many adjustment variables without a clear meaning about the experimental

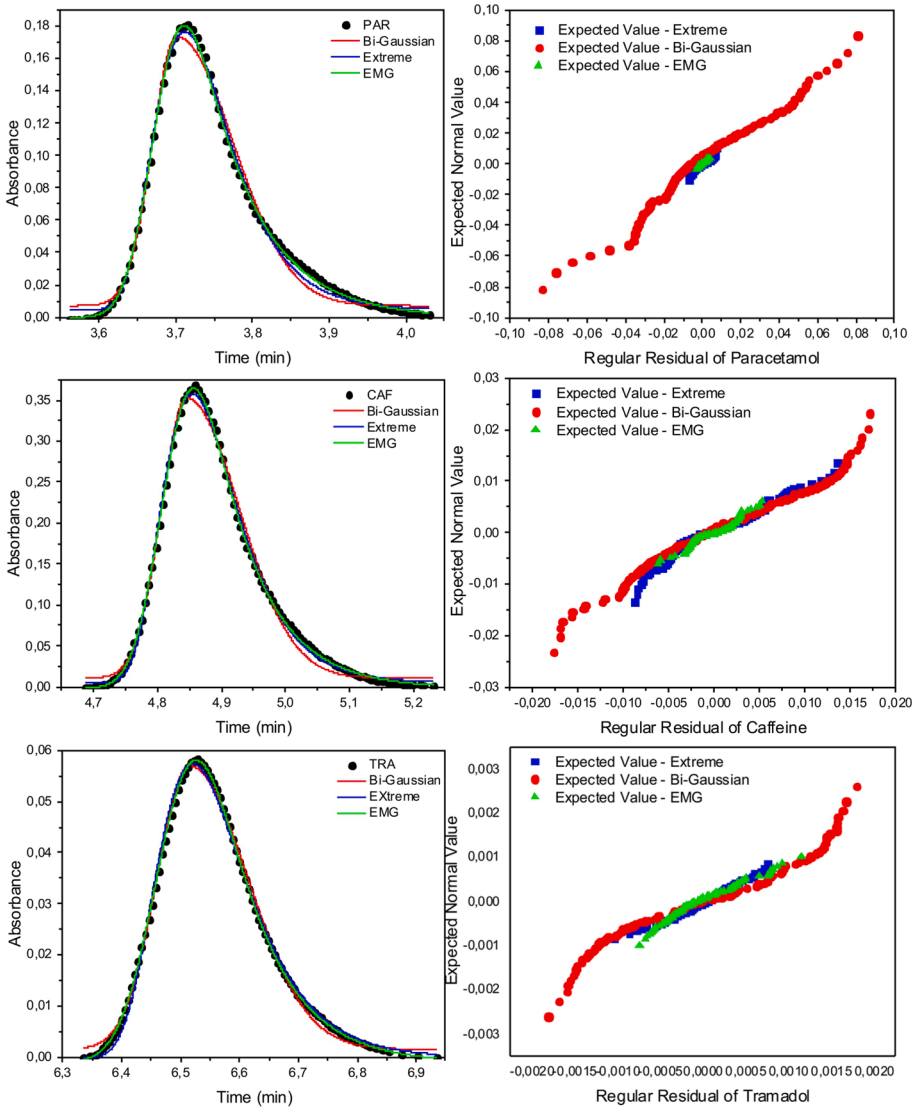

Fig. 1. (A-Left) Selected chromatographic peaks and the corresponding peak profiles obtained with the three models. (B-Right) Typical Q-Q plots of the residuals for the theoretical models and three selected analytes. (PAR, CAF, and TRA refer to paracetamol, caffeine, and tramadol, respectively).

chromatographic parameters, representing a significant drawback for their use in chromatography. The remaining three distributions, Bi-Gaussian (based on four variables), EMG (involving four variables) and Gumbel (defined by three variables), provided good fits of the peak shape for all experimental chromatographic parameters assayed within the whole range of values covered as stated in Experimental (Fig. 1). The Gumbel equation, $y = Ae^{\left(-e^{\left(-\frac{t-t_{max}}{w}\right)}-\left(\frac{t-t_{max}}{w}\right)+1\right)}$, involves the following three variables: location of the peak t_{max}, the peak width w ($= \frac{\sqrt{6}\sigma}{\pi}$) (being σ the standard deviation of the peak), and amplitude A, easily derived from the chromatographic peak.

Fig. 1A shows comparative settings of the best three models to the experimental chromatographic peaks of three analytes under the experimental conditions selected as reference (section 2.4), whilst Fig. 1B shows the typical probability plots of the residuals (Q-Q plots). The Q-Q plots indicate that the error terms in modelling the chromatographic peak shapes show a normal distribution, particularly for the Gumbel and EMG models. The Q-Q plots in Fig. 1B and the statistical parameters included in Table 1 confirm the general goodness of fit of the three models for the three analytes taken as reference. Nonetheless, similar reliability also achieved the rest of the analytes, even with those using the acetonitrile-based mobile phase (Fig. SI-3). As a result, we can state that the Gumbel model can successfully model the chromatographic peak profiles.

Notwithstanding, to check the suitability of the proposed Gumbel distribution for modelling the chromatographic peak shape and provide proper chromatographic parameters, we compared the values of some parameters derived from the experimental peaks obtained under different analytical situations with those theoretically calculated from each distribution model. Fig. 2 shows the results for three analytes, although the other drugs have similar behaviour. Thus, we found that the theoretical values of all areas calculated according to the best three models fall inside the prediction bands deduced from the experimental data as a function of the analyte concentration (Fig. 2A). However, a plot of the experimental and theoretical retention times (Fig. 2B) and the peak widths (Fig. 2C, D) against the analyte concentration, pH and mobile phase composition confirms several minor differences between the models, although with some advantages for the Gumbel distribution.

To summarise, as a whole, the fit of the peak shape with the EMG and Bi-Gaussian models deteriorates and improves, respectively, for long retention times, while the Gumbel distribution works appropriately. Furthermore, better suitability of the Gumbel and EMG distributions was possible working at high concentrations of the analytes (Fig. 2B). Similarly, we obtained better predictions of the peak widths with the Gumbel distribution for a wide pH range and low-medium %MeOH of the mobile phase (Fig. 2C, D). In general, the Gumbel distribution compared favourably against the other two models, not about the peak area, which resulted similarly, but for the retention times and peak widths, particularly for lower flow rates, higher pHs and longer retention times. Additionally, the three variables of the Gumbel model can be derived directly from the chromatographic peaks, contrarily to those involved in the Bi-Gaussian and EMG distributions.

Further, the number of points needed for a good fit, mainly those found at the peak tailing, affects the fitting firmly using Bi-Gaussian and EMG but not using Gumbel. Thus, if we try to fit peaks with tails containing a large number of points, Bi-Gaussian converges to a logistic function, while if there are few points in the front of the peak, EMG does not converge all. Conclusively, the versatility of the Gumbel model provides good support and prediction possibilities for different analytes and mobile phases, especially for the peak area (Fig. 2A) and the retention time (Fig. 3A).

Apart from fitting the peak shape, a possible theoretical evaluation of the retention time based on some experimental chromatographic parameters is of concern. We studied the combined effect of the mobile phase composition (%MeOH), pH, phosphate concentration, and flow rate (FR) on the retention time. The experimental data pool from each analyte fitted to an exponential equation containing the same terms as the variables studied. As an example, we include the three following equations for three analytes; although similar equations are possible for the other drugs,

$$t_R = (17.30 \pm 0.60)e^{(-1.94\pm0.11)FR} + (13.03 \pm 1.40)e^{(-0.06\pm0.01)(\%MeOH)} \quad (\text{with } R^2 = 0.9920;\ \text{for paracetamol}) \tag{1}$$

$$t_R = (23.50 \pm 0.90)e^{(-1.95\pm0.08)FR} + (82.80 \pm 8.80)e^{(-0.10\pm0.01)(\%MeOH)} \quad (\text{with } R^2 = 0.9920;\ \text{for caffeine}) \tag{2}$$

$$t_R = (31.34 \pm 20.00)e^{(-3.00\pm2.00)FR} + (238.53 \pm 50.00)e^{(-0.09\pm0.01)(\%MeOH)} + (2.11 \pm 0.25)pH + (-10.39 \pm 3.00) \quad (\text{with } R^2 = 0.9770;\ \text{for tramadol}) \tag{3}$$

As expected, we found that the contribution of each parameter is different for each analyte, although the flow rate (*FR*) and the mobile phase composition (% MeOH) contributes similarly for analytes with similar characteristics. However, the contribution from pH was not statistically significant for analytes showing minor acidic characters, such as paracetamol and caffeine. At the same time, the effect of the phosphate concentration was negligible for all analytes, probably due to the stabilising effect of the ionic strength.

We evaluated the goodness of fit of the above equations statistically by plotting the theoretical retention times ($t_{R\ cal}$) calculated from Eqs. (1)–(3) *versus* the corresponding experimental retention times ($t_{R\ exp}$) (Fig. 3A). The plot of the data for each analyte fits well to a straight line ($t_{R\ cal} = a + m\, t_{R\ exp}$), according to the high coefficients of determination ($R^2 > 0.9905$) and the values of the theoretical slopes ($m = 1$) and intercepts ($a = 0$), which fall within the corresponding confidence interval of the fits.

Table 1
The goodness-of-fit of the three theoretical models to the peak shapes of three analytes under the selected reference chromatographic conditions using five statistic parameters (AIC: Akaike Information Criterion; BIC: Bayesian Information Criterion).

Model	AIC	BIC	Adj. R-Square	Residual Sum of Squares	Reduced Chi-Sqr
Tramadol					
Extreme	−1634,39	−1621,83	0,9997	1,19E-5	1,21E-7
EMG	−1596,21	−1581,27	0,9995	1,69E-5	1,72E-7
Bigaussian	−1399,48	−1384,55	0,9966	1,14E-4	1,17E-6
Caffeine					
Extreme	−1233,83	−1220,46	0,9977	0,00342	2,97E-5
EMG	−1421,94	−1406,02	0,9995	6,91E-4	6,06E-6
Bigaussian	−1103,88	−1087,96	0,9932	0,01001	8,78E-5
Paracetamol					
Extreme	−1156,64	−1143,92	0,9955	0,00175	1,72E-5
EMG	−1357,69	−1342,56	0,9993	2,57E-4	2,55E-6
Bigaussian	−709,75	−694,62	0,9880	0,11607	0,00115

3.2. Modelling of the effect of quantum parameters

Deep knowledge about the structural and quantum parameters of the analytes is beneficial for a better understanding of the chromatographic retention process. The main difference between both groups of analytes relates to the much greater dipolar moment of the first group of analytes (Table SI-2), which are easily separated using methanol. Contrarily, the analytes of the second group separate better with the less polar mobile phase based on acetonitrile. However, the parameters governing the separation of the analytes of each group encompass the simultaneous action of the molecule size, the conjugated system and the acidity of the functional groups capable of interacting with the mobile phase.

Paracetamol and caffeine are planar neutral molecules with a

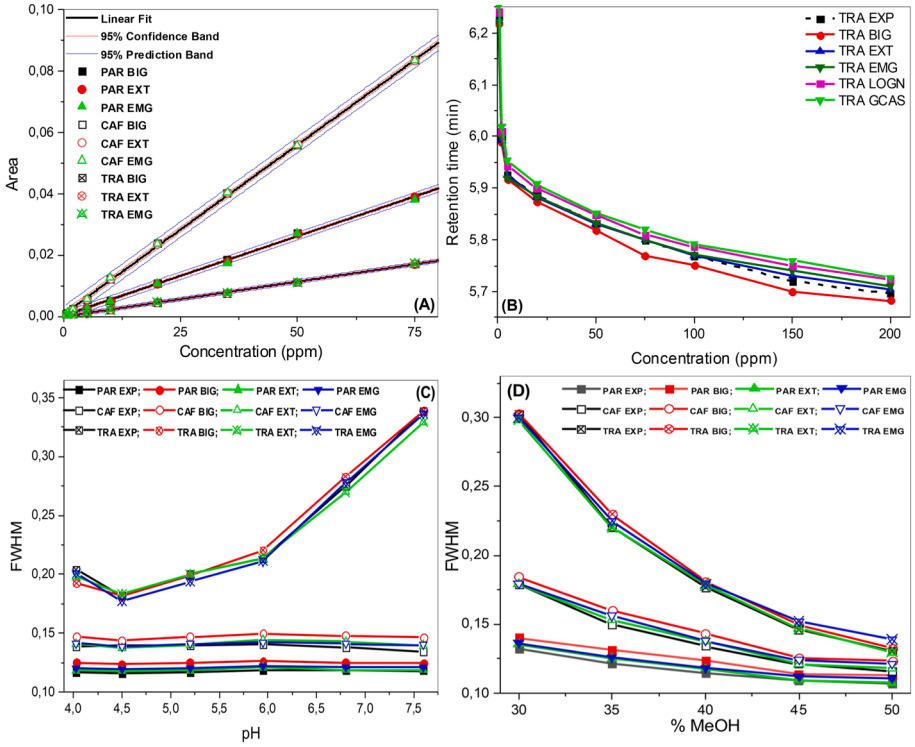

Fig. 2. Comparative plots between: (A) peak areas, (B) retention times, and (C,D) FWHMs against (A,B) concentration, (C) pH, and (D) % MeOH. (EXP: experimental data; BIG: Bi-Gaussian; EXT: Extreme (Gumbel); EMG: Exponential Modified Gaussian: other symbols as in Fig. 1).

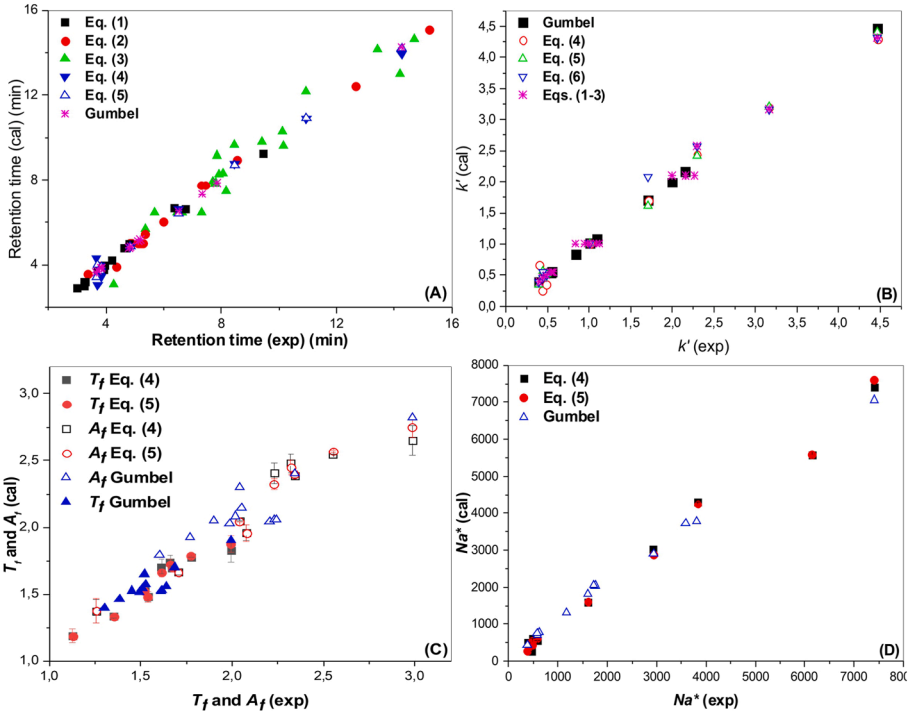

Fig. 3. (A) Theoretical retention times from Eqs. (1)–(5) and the Gumbel model *vs* the experimental retention times. (B) Theoretical capacity factors (k'_{cal}) from Eqs. (4)–(6) and from the Gumbel model and Eqs. (1)–(3) *vs* the experimental capacity factors (k'_{exp}). (C) Theoretical values of T_f, A_f from Eqs. (4), (5) and the Gumbel model *vs* the experimental values. (D) Theoretical values of N_a* from Eqs. (4), (5) and the Gumbel model *vs* the assumed experimental values. (The plots in Fig. 3 correspond to paracetamol, caffeine, and tramadol, but we obtained similar agreement between the theoretical and experimental values for the other analytes).

relatively sizeable conjugated system. Similarly, salicylic acid also has a planar conjugated cyclic structure due to the formation of an intramolecular H-bond since it is in the ionised form within the pH range covered (pH 4.0–8.0). Contrarily, tramadol has a larger size with various conformational structures owing to the free rotation around the C1″-C2 single bond. Paracetamol has four potential conformers: *trans-E*, *trans-Z*, *cis-E* and *cis-Z*, depending on the orientation of the amino and the OH groups. However, only the two conformers *trans* are very stable in solution, with similar energy and an open structure that facilitates solvation.

On the other hand, the tramadol sample here is an equimolecular mixture of the 1R,2R and 1S,2S enantiomers, but the quantum

parameters of both enantiomers have similar energy and consequently identical energetic behaviour. Any molecular structure of tramadol is in the deprotonated form beyond the pH range covered. In any case, the leading quantum parameters of its neutral structures show values smaller than the protonated ones, according to the data calculated by the Kohn-Sham DFT (Table 2). The other analytes of this group (phenylephrine, atenolol, acebutolol, nadolol, and propranolol) have a large chain attached to a conjugated cyclic structure. Some of the other analytes here are also chiral compounds, but we occasionally refer to this circumstance because the stationary phase does not show chiral properties.

Molecular quantum parameters, such as the non-polar (hydrophobic) surface area and the solvent accessible surface (SAS) (Table 2, Table SI-2), showed a direct positive relationship with the retention times for some analytes. Contrarily, the dipole moment (μ), polarizability (α), polar molecular surface (SEP) and SEP/SAS ratio showed an inverse relationship, working under the selected reference experimental conditions (section 2.4). However, other quantum parameters in isolation show quadratic relationships. The effect of each quantum parameter taken individually does not show the same relationship with all analytes. For this reason, we use them in combination. Thus, by correlation analysis and using all the experimental data obtained for the whole pH range covered (4.0–8.0), we deduced the following two more general equations, each one useful for calculation several chromatographic parameters for paracetamol, caffeine, and tramadol,

$$y = a_o + a(\mathrm{GAP}) + b\mu + c\mu^2 \quad (\text{for } t_R,\ k',\ T_f,\ A_f,\ N_a{*}) \tag{4}$$

and

$$\begin{aligned} &y = a_o + a(\mathrm{GAP}) \quad (\text{for } t_R,\ k',\ N_a{*}) \\ &\text{or} \\ &y = a_o + a\mu \qquad (\text{for } T_f,\ A_f) \end{aligned} \tag{5}$$

where the term y represents any of the following parameters: the retention time t_R, the capacity factor k', the tailing factor T_f ($= (A_{0.1} + B_{0.1})/2A_{0.1}$), the asymmetry factor A_f ($= B_{0.1}/A_{0.1}$) or the theoretical plates number $N_a{*}$. The numerical values for the coefficients a_o, a, b and c are shown in Table 3 for each equation and parameter, while the GAP and μ values are in Table 2. The theoretical values calculated for t_R and k', using Eqs. (4), (5) agree very well with the corresponding experimental values (Fig. 3A, B). On the other hand, the theoretical values for T_f, A_f and $Na{*}$ fit well with those deduced from the experimental chromatographic peaks and the Gumbel distribution (Fig. 3 C, D). We also calculated the experimental values for the number of theoretical plates using the well-accepted equation [22], $N_a^* = \frac{41.7 \cdot \left(\frac{t_R'}{w_{0.1}}\right)^2}{\frac{B_{0.1}}{A_{0.1}} + 1.25}$. It is worth remarking that Eqs. (4), (5) provided statistically similar results for each quantum parameter evaluated, which means a strong correlation between them, as noted in the corrplot graph (Fig. 4A). Thus, GAP, α, SAS and SEP are directly interrelated (GAP, α, and SAS positively, whilst SEP negatively). So, only one of them should be in the correlation analysis. Contrarily, the dipole moment acts as a second independent parameter. Using Principal Component Analysis (PCA), we reached similar conclusions (Fig. 4B), with the PCA1

Table 3
Equations corresponding to Eqs. (4), (5), obtained from the correlation analysis, and the corresponding values for their coefficients. (PAR: paracetamol, CAF: Caffeine, TRA: tramadol, GAP: energy band gap, μ: dipole moment).

Eq. (4); Two quantum parameters*	Eq. (5); One quantum parameter**
$\boldsymbol{tr = a_o + a\ GAP + b\ \mu + c\ \mu 2}$	$\boldsymbol{tr = a_o + b\ GAP}$
$a_o = -162.1015 \pm 19.3244$	$b = -37.103 \pm 1.357$
$a = 7.5313 \pm 0.7960$	$a_o(\mathrm{CAF}) = 273.475 \pm 9.828$
$b = 40.6414 \pm 4.8963$	$a_o(\mathrm{PAR}) = a_o(\mathrm{CAF}) - 39.054 \pm 1.408$
c = -3.1154 ± 0.3744	$a_o(\mathrm{TRA}) = a_o(\mathrm{CAF}) + 217.515 \pm 7.770$
$\boldsymbol{k' = a_o + a\ GAP + b\ \mu + c\ \mu 2}$	$\boldsymbol{k' = a_o + b\ GAP}$
$a_o = -58.2596 \pm 8.1885$	$b = -13.3145 \pm 0.5387$
$a = 2.7046 \pm 0.3373$	$a_o(\mathrm{CAF}) = 97.4086 \pm 3.9014$
$b = 14.3590 \pm 2.0748$	$a_o(\mathrm{PAR}) = a_o(\mathrm{CAF}) -14.1630 \pm 0.5590$
c = -1.1026 ± 0.1587	$a_o(\mathrm{TRA}) = a_o(\mathrm{CAF}) + 78.0847 \pm 3.0842$
$\boldsymbol{T_f = a_o + a\ GAP + b\ \mu + c\ \mu 2}$	$\boldsymbol{T_f = a_o + b\ \mu}$
$a_o = -9.01105 \pm 4.07343$	$b = -1.5451 \pm 0.4858$
$a = 0.38325 \pm 0.16779$	$a_o(\mathrm{CAF}) = 7.6695 \pm 1.9380$
$b = 2.78798 \pm 1.03210$	$a_o(\mathrm{PAR}) = a_o(\mathrm{CAF}) + 7.3869 \pm 2.2516$
c = -0.21070 ± 0.07892	$a_o(\mathrm{TRA}) = a_o(\mathrm{CAF}) + 10.4966 \pm 3.3343$
$\boldsymbol{A_f = a_o + a\ GAP + b\ \mu + c\ \mu 2}$	$\boldsymbol{A_f = a_o + b\ \mu}$
a_o = -19.0104 ± 8.1517	b = -3.0887 ± 0.9726
$a = 0.7661 \pm 0.3358$	$a_o(\mathrm{CAF}) = 14.3341 \pm 3.8796$
$b = 5.5732 \pm 2.0654$	$a_o(\mathrm{PAR}) = a_o(\mathrm{CAF}) + 14.7665 \pm 4.5076$
c = -0.4212 ± 0.1579	$a_o(\mathrm{TRA}) = a_o(\mathrm{CAF}) + 20.9823 \pm 6.6749$
$\boldsymbol{Na{*} = a_o + a\ GAP + b\ \mu + c\ \mu 2}$	$\boldsymbol{Na{*} = a_o + b\ GAP}$
$a_o = -99476.4 \pm 15627.7$	$b = -22460 \pm 2130$
$a = 4668.9 \pm 643.7$	$a_o(\mathrm{CAF}) = 164214 \pm 15422$
$b = 24351.5 \pm 3959.6$	$a_o(\mathrm{PAR}) = a_o(\mathrm{CAF}) -24103 \pm 2210$
c = -1872.0 ± 302.8	$a_o(\mathrm{TRA}) = a_o(\mathrm{CAF}) + 131993 \pm 12192$
* Particular equations valid for the three compounds, replacing the corresponding values for *GAP* and μ from Table 2.	** Particular equations valid for the three compounds, using a different intercept in each case but the same slope. Values for *GAP* and μ are from Table 2.

Table 2
Various quantum chemical parameters, calculated through the Kohn-Sham DFT for three drugs at different pH conditions. The arrows linked to the tramadol name refer to the more (↑) and less (↓) active conformer. The values of the top nine rows correspond to a situation where all possible species of each drug could be present simultaneously in the solution. Contrarily, the values of the eight rows below correspond to the situation where only one single chemical species of each drug exists in the solution.

Molecule	pH	ΔE (GAP) (eV)	μ (Db)	α_{ave} (Å^3)	SAS (Å^2)	SEP (Å^2)
Paracetamol	4.5	6,210	8,670	16,240	326,880	104,840
Paracetamol	6.8	6,214	8,629	16,245	326,852	104,855
Paracetamol	7.2	6,219	8,590	16,252	326,826	104,868
Paracetamol	7.6	6,226	8,531	16,263	326,788	104,887
Caffeine	4.5	7,240	3,980	18,220	350,819	92,784
Tramadol	4.5	13,060	10,990	28,870	483,810	52,370
Tramadol	6.8	12,999	10,897	28,862	483,805	52,352
Tramadol	7.2	12,939	10,801	28,851	483,796	52,335
Tramadol	7.6	12,850	10,658	28,835	483,782	52,309
Paracetamol	Neutral	6,701	4,780	16,960	324,300	106,133
Paracetamol	Protonated	6,209	8,667	16,237	326,878	104,842
Caffeine	Neutral	7,238	3,983	18,219	350,819	92,784
Caffeine	Protonated	7,273	9,879	17,442	352,705	94,180
Tramadol ↑	Neutral	6,928	3,032	26,222	453,393	46,785
Tramadol ↑	Protonated	7,567	6,699	27,342	461,696	49,559
Tramadol ↓	Neutral	7,101	1,448	27,801	482,893	50,633
Tramadol ↓	Protonated	13,059	10,992	28,873	483,814	52,369

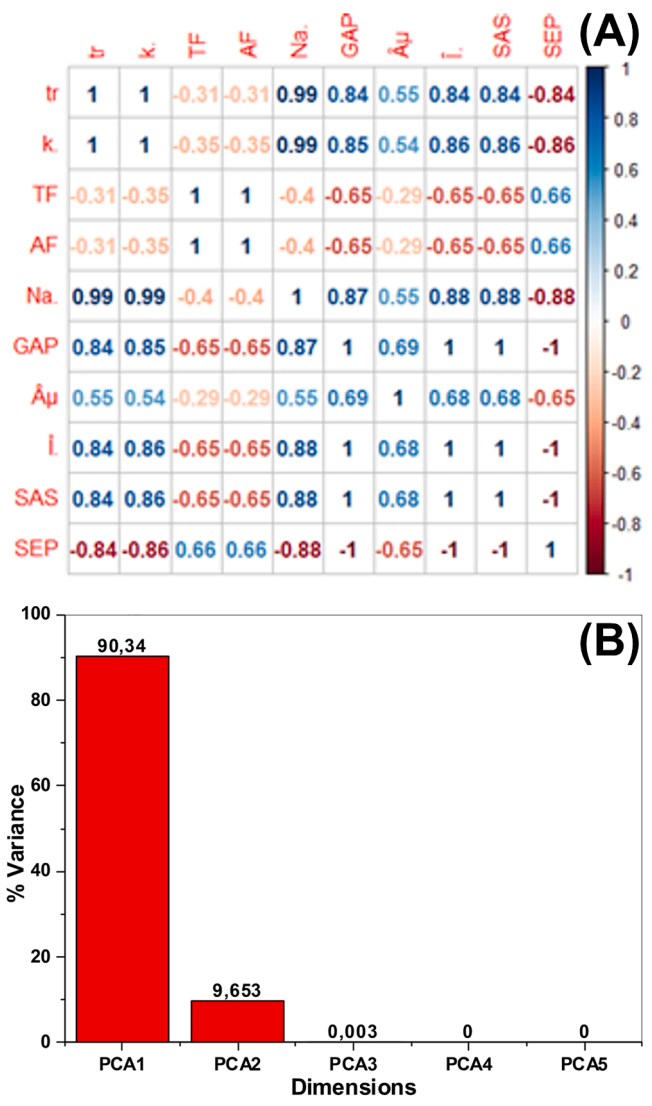

Fig. 4. (A) Corrplot graph containing the correlation found between variables. (B) Scree plot representing the relative contribution of the principal components. (t_r: retention time; k. (k'): capacity factor; TF (T_f): tailing factor; AF (A_f): asymmetry factor; Na (Na^*): number of theoretical plates; GAP (ΔE): energy bandgap; (μ): dipole moment; (α): polarizability; (SAS): solvent accessible surface; (SEP): polar molecular surface.

explaining 90% variance and covering the 99.99% variance with the PCA2. In other words, only two parameters would be adequate for a statistically complete explanation at the 5% significance level, under the pH range conditions stated (4.0–8.0).

Notwithstanding, to understand the combined effect of the quantum parameters under the selected experimental reference conditions (section 2.4), we joined the global effect of four molecular quantum parameters with values ranging as stated in Table 2 to develop a theoretical equation for the capacity factor. This combination resulted in the following general equation, valid for paracetamol, caffeine and tramadol in the pH range covered,

$$Logk' = (193.50 \pm 3.00) - (0.19 \pm 0.01)\mu - (4.82 \pm 0.17)\alpha + (0.02 \pm 0.05)(SAS) - (1.13 \pm 0.09)(SEP) \quad (6)$$

with a high coefficient of determination ($R^2 = 0.9886$). Eq. (6) allows us to calculate the capacity factor of each analyte by replacing the symbol of the quantum parameter with its corresponding value from Table 2. We evaluated the goodness of fit of the above equation by plotting the theoretical capacity factors calculated from Eq. (6) *versus* the experimental capacity factors derived from the chromatograms (Fig. 3B). We obtained a straight line ($R^2 = 0.9903$) with a slope (0.98 ± 0.02) very close to unity, and all the theoretical values falling inside the 95% prediction bands (Fig. 3B). Eq. (6) shows that the contribution of the parameter SAS is minimum, while the three parameters, μ, α, and SEP, participate negatively.

To achieve a possible generalisation of this evaluation, we developed alternative equations for the capacity factor, including eight quantum parameters (Table SI-2), all the analytes assayed under the pH range covered and using the methanol–water and acetonitrile–water mixtures as mobile phases. We achieved the following equations for each mobile phase,

$$Logk' = (14.288 \pm 1.400) - (4.240 \pm 0.200)(GAP) - (0.752 \pm 0.050)\mu + (0.193 \pm 0.020)\alpha + (0.024 \pm 0.010)(SAS) - (0.453 \pm 0.030)(SEP) + (107.018 \pm 9.000)(SEP/SAS) - (0.003 \pm 0.001)(VPOT\_X) - (0.307 \pm 0.040)(VPOT\_H)(\text{with } R^2 = 0.9880) \quad (7)$$

using the methanol-based mobile phase and the numerical values of the quantum parameters included in Table SI-2. However, it is worth noting that removing the contribution of some quantum parameter, such as the two electrostatic potentials, the contribution of the remaining parameters changes, and the fit worsens, as indicated in the following equation,

$$Logk' = (-15.244 \pm 1.800) + (0.214 \pm 0.030)(GAP) + (0.001 \pm 0.0003)\mu - (0.078 \pm 0.090)\alpha + (0.034 \pm 0.050)(SAS) - (0.093 \pm 0.080)(SEP) + (39.367 \pm 3.000)(SEP/SAS)(\text{with } R^2 = 0.9690) \quad (7a)$$

Simultaneously, using an acetonitrile-based mobile phase and the corresponding numerical values of Table SI-2, we also performed a similar fit. In this case, the two following equations, including or excluding the effect of the electrostatic potentials, were obtained,

$$Logk' = (2640.974 \pm 32.200) - (33.793 \pm 2.200)(GAP) - (8.792 \pm 0.400)\mu - (2.863 \pm 0.300)\alpha - (4.166 \pm 0.200)(SAS) + (22.164 \pm 2.900)(SEP) - (11716.105 \pm 110.200)(SEP/SAS) + (0.050 \pm 0.020)(VPOT\_X) + (0.232 \pm 0.030)(VPOT\_H)(\text{with } R^2 = 0.9812) \quad (8)$$

$$Logk' = (-148.678 \pm 11.700) + (1.753 \pm 0.300)(GAP) + (0.356 \pm 0.050)\mu - (0.057 \pm 0.030)\alpha + (0.256 \pm 0.040)(SAS) - (1.171 \pm 0.300)(SEP) + (639.309 \pm 38.900)(SEP/SAS)(\text{with } R^2 = 0.9668) \quad (8a)$$

As stated above, to confirm the validity of these equations, we fit the k' theoretical values, calculated through Eq. (7) and Eq. (8), *versus* the k' experimental values (Fig. 5). As before, the correspondence between both values, theoretical and experimental, confirms the validity of the developed equations. (The coefficients of Eqs. (7, 7a, 8 and 8a) show rounded numbers. The loss of some digits causes an error due to the very close values of the quantum parameters, Table SI-2. The original coefficients are in Table SI-3).

As a result of Eq. (7) and Eq. (8), we can state that the parameters α,

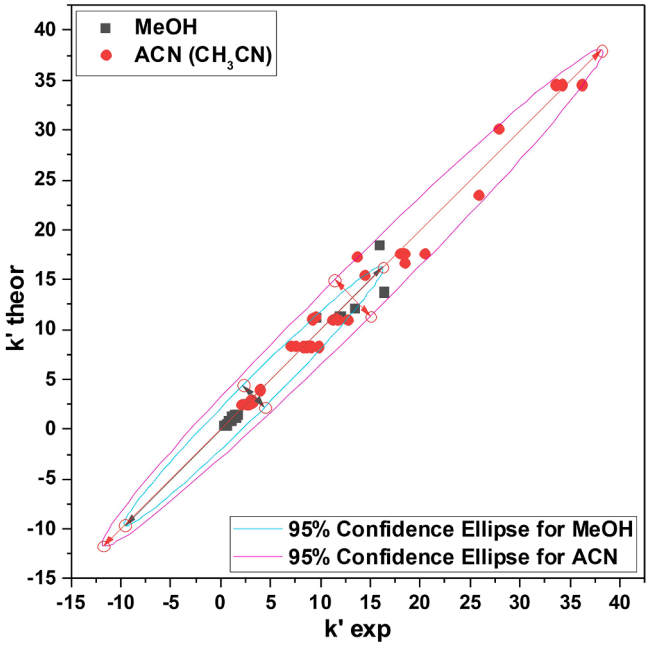

Fig. 5. Theoretical capacity factors (k'_{cal}) from Eq. (7) and Eq. (8) *vs* the experimental capacity factors (k'_{exp}) for the mobile phases based on methanol (MeOH) and acetonitrile (ACN).

SAS, SEP, SEP/SAS, VPOT_X, and VPOT_H contribute in an opposite sense, depending on the mobile phase considered, although GAP and μ act negatively in both situations. However, they all contribute to a different extent. Thus, we can arrive at the following general conclusions from this section. First, the effect of each quantum parameter is a consequence of the interconnection with those from the others; second, increasing the number of quantum parameters improves fitting; and third, the electrostatic potential at atomic sites provides practical utility as a reactivity index for the process of hydrogen bonding between the drugs and the mobile phase, in agreement with the ideas previously reported [26]. In other words, the physicochemical interpretation of the contribution of each quantum parameter is complex because it depends on the number of analytes and parameters considered in the calculation. This dependence probably links to the interrelationship between them, which also changes with the assayed experimental conditions.

3.3. Structure-retention relationships

The analytes chromatographed using methanol–water as a mobile phase have a pK_a value above 9.0 except salicylic acid (pK_a: 2.97). Nonetheless, these values should be nominal, and some deviations are possible depending on the structural and dielectric properties of the solvent [48] and the possible presence of ions (ionic strength) [49]. Methanol in water can facilitate intra- and inter-molecular H-bonds, as previously stated comparing Eqs. (7) and (7a) ((8) and (8a) for the acetonitrile case), but regulated by the solvent mixture composition and molecular parameters, such as dielectric properties and dipole moment [50]. In consequence, the acidity of the solutes and their chromatographic behaviour change. The reason is that the acid dissociation constant K_a ($=K_i\,K_d$) results from an overall process involving two other constants, the ionisation constant K_i and the dissociation constant K_d of a possible ion-pair association formed. The molecular structure of the association formed governs the K_i constant, while the dielectric constant of the solvent mixture acts mainly on K_d.

All the drugs of the first group separated with a mobile phase based on methanol have an aromatic system contributing to their lipophilic character. Some of them behave as β-blockers, containing an alkanol amine group responsible for their alkaline physicochemical properties. Further, atenolol and acebutolol also have an amide function in a lateral chain of the aromatic system. The most appropriate experimental conditions for separating these analytes change with the pH of the mobile phase, as stated for the capacity factor (Fig. 6). Differences in their behaviour particularly relate to the size of the whole molecule (steric effects) and the aromatic system (planarity) modulated by the functional groups present in the lateral radicals. However, among the various quantum molecular descriptors stated in the experimental, only a combination of a few were more directly involved in the chromatographic behaviour of the analytes.

The frontier molecular orbitals (HOMO and LUMO) are the most critical delocalised boundaries surfaces of an organic molecule for predicting reactive position in conjugated systems. In general, the negatively charged heteroatoms, π bonds and phenyl rings constitute the HOMO regions, which are therefore the most probable sites for retention. In this way, molecules having high E_{HOMO} and low E_{LUMO} are prone to better interactions and the frontier orbital gap ΔE(GAP) ($=E_{LUMO}–E_{HOMO}$) is the quantum parameter generally used for a theoretical evaluation of the chemical reactivity and kinetic stability of a molecule. Thus, a molecule with a small frontier orbital gap would show better retention, also facilitating polarizability. However, theoretical data of the selected drugs reported in Table 2 do not support faithfully this statement, suggesting strong additional participation of other structural parameters. For example, the protonated forms of tramadol in the N atom have values for ΔE higher than for paracetamol and caffeine.

Nonetheless, the neutral conformers of the tramadol species have the smallest values for ΔE (Table 2), thus improving their retention. The different energy levels between the conformers of tramadol suggest that the frontier molecular orbitals steric factors play an essential role in the retention process. Fig. 7A shows the large spatial region occupied by the HOMO region, located all over the neutral tramadol molecule in the more active conformer (tramadol ↑), thus facilitating its retention. This spatial proximity between the LUMO and HOMO orbitals only occurs for the most active conformer (tramadol ↑), but not for the one with less energy (tramadol ↓) (Fig. 7A). The spatial proximity of the HOMO and LUMO frontier orbitals requires closeness of the amino and benzene groups (Fig. 7), representing an energetically unfavourable situation but sterically favourable. This steric factor is less critical in caffeine and much less still in paracetamol, where the frontier orbitals do not cover the vicinity parts of the molecule (Fig. 7). The contribution of the steric factor is also present in other analytes (Fig. SI-4). For example, phenylephrine in protonated form is the most abundant protomer in the pH range covered with an intermediate HOMO-LUMO bandgap value among all the drugs studied but a localised HOMO on only the phenyl group. In addition, the LUMO localises on the opposite side of the molecule. This steric factor could be one reason for the low retention of phenylephrine shown in Fig. SI-1. On the other hand, ibuprofen (in both neutral and deprotonated forms) presents very different proximity between HOMO and LUMO, and it confirms the low retention of this drug.

From the structural point of view, the most different compound of this first group is salicylic acid with a pK_a 2.97. However, within the pH range assayed, salicylic acid is therefore in the ionised form (Fig. SI-5) with lower internal energy and a strengthened acidity. This situation alters the geometrical and electronic properties, lengthening the double and O–H bonds and shortening the single and H···O bonds. This behaviour facilitates forming an intramolecular H-bond (O–H···O) between the carbonyl and the hydroxyl groups, generating a new π-conjugated ring in the molecule, especially at high pHs. This expansion in the conjugated system strengthen the H-bond by resonance and charge delocalisation, but the aromatic system weakens [51,52], which strongly decreases retention (Fig. 6).

In summary, under acidic conditions, heteroatoms outside a conjugated system would be protonated, as is the case of tramadol, propranolol, acebutolol, and other amino compounds, decreasing retention capability, although in a different extension. On the contrary, under alkaline conditions, the amount of deprotonated (neutral) molecules

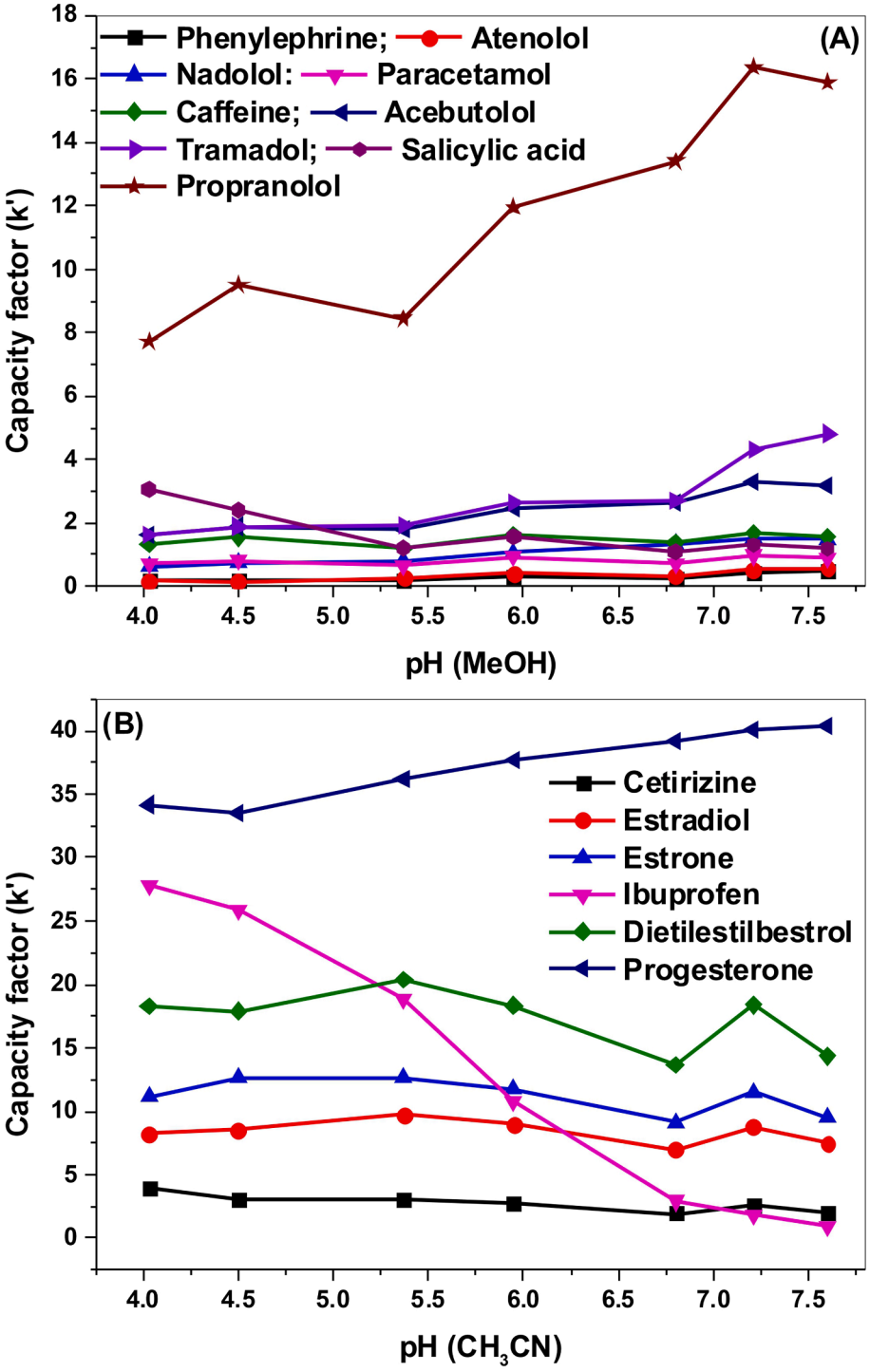

Fig. 6. Capacity factor *vs* pH for the analytes chromatographed with (A) methanol-, and (B) acetonitrile(CH_3CN)-based mobile phases.

grows for tramadol, propranolol, and other similar compounds, thus facilitating retention. Tramadol and structurally similar drugs behave as a base compound, which in acidic solution would be physisorbed on the stationary phase. However, at basic pHs, the deprotonated N atoms of tramadol, with free lone electrons pair, facilitate a chemisorption process. The two neutral molecular conformers of tramadol would be involved in the retention process, but with different efficacy, because one of them (tramadol ↑) requires an acute angle of attack while the other conformer (tramadol ↓) obtuse. The small molecular size and neutral structure of the paracetamol and caffeine molecules support a retention process involving π interactions, slightly altered by their dipole moments and SAS values.

The acidity of paracetamol is minimal because the amine group is inside a conjugated system and the OH group shows a high pK_a value (pK_a = 9.38) [53], a result of the moderately activating acetamide group. A similar but more pronounced behaviour stands out for propranolol, whose capacity factor grows with pH (Fig. 6). This relationship shows the strong basicity of propranolol, which suggests an involvement of the hydroxyl and amino groups in its retention. Similarly, the absence of OH groups in caffeine supports an even much smaller basicity character. On the contrary, salicylic acid shows the opposite behaviour. The above results support tramadol-like or propranolol-like behaviour for

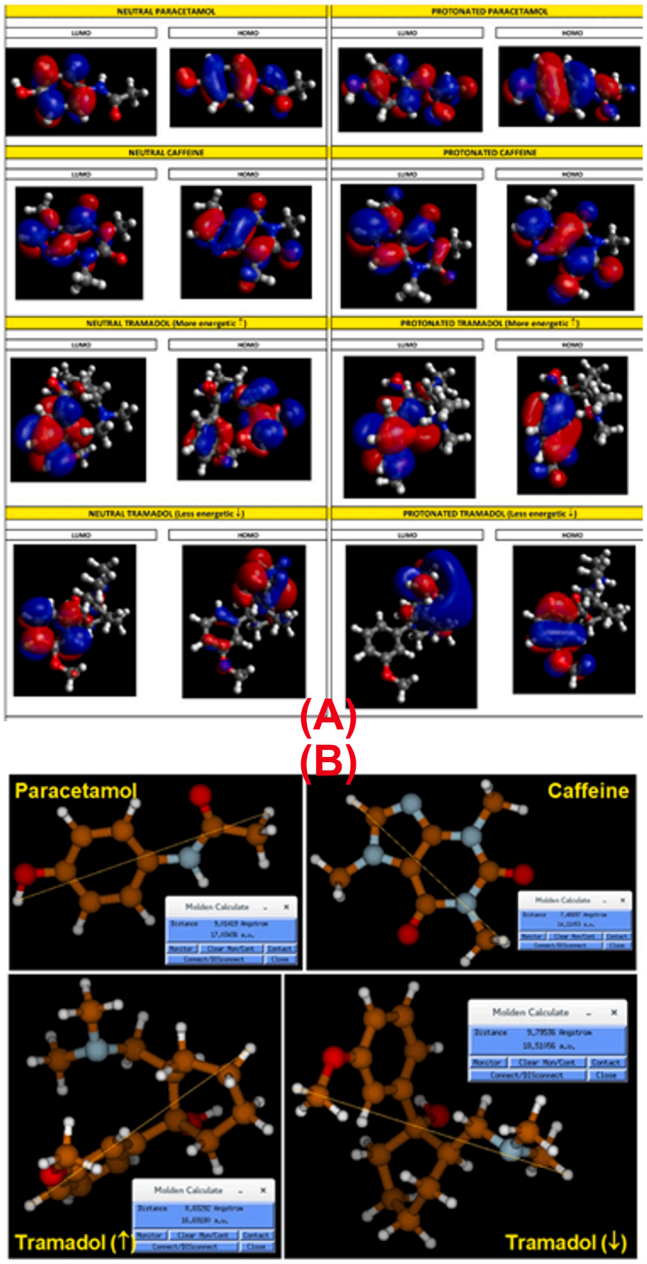

Fig. 7. (A) Representation of the HOMO and LUMO molecular orbitals for paracetamol, caffeine, and tramadol. (B) A comparison of the molecular size of three selected analytes. The lobes in red represent bonding orbitals, whiles those in blue anti-bonding orbitals.

molecules containing a particular basicity character, although modulated by steric factors through a planar conjugated system. On the contrary, behaviours similar to paracetamol and salicylic acid would result in neutral and acidic molecules, respectively, with planar conjugated systems.

Similar arguments rise for explaining the chromatographic behaviour of the analytes of the second group separated by acetonitrile–water as a mobile phase. These analytes represent three steroidal and three nonsteroidal molecules, all characterised by a dipole moment much smaller than the drugs of the first group (Table SI-2). These compounds have pK_a values above 9.0 except cetirizine (pK_a: 1.52, 2.92, 8.27) and ibuprofen (pK_a: 5.2), similar to those of the drugs of the first group. However, this coincidence in the pK_a values and the chromatographic discrepancies with the analytes of the first group means that parameters other than pK_a support the primary retention mechanism. The main geometrical characteristic of the analytes of this group is their sizeable molecular size, probably excluding diethylstilbestrol and ibuprofen. Compared with their molecular size, the aromatic system of all these compounds is small, just an isolated benzene ring except cetirizine and diethylstilbestrol (DES). There is no clear relationship between the capacity factor and the quantum parameters of the analytes of this group. According to their chromatographic behaviour, it is reasonable to think that elution occurs primarily due to a combination of the little dipole moment linked to a larger molecular size and the acidic character of the molecule.

Cetirizine leaves fast the column, probably due to a lack of rigidity in the molecule, a relatively large size, similar to the other drugs of this group, and a carboxylic group (pK_a: 2.92). However, cetirizine exists as a zwitterion in the pH covered, although generating folded conformers of low polarity due to an intramolecular charge neutralisation [54]. Contrarily, the ibuprofen molecule is smaller and contains a carboxylic group but leaves the column much later at acidic pHs, linking to the possible formation of stronger dimers than cetirizine. However, ibuprofen leaves the column the first at basic pHs (7.6) (Fig. 6, Fig. SI-1), probably due to the destruction of the dimers. Estradiol, estrone and progesterone contain a rigid structure with four condensed cycles. However, differences in their separation refer fundamentally to the smaller size of the aromatic system in progesterone (less planar molecule) and the acetyl group in position 17 (D ring), which replaces the hydroxyl and ketone functions of estradiol and estrone, respectively.

Further, the acetyl group of progesterone becomes an enol function facilitated under alkaline conditions. The estrone behaviour is intermediate, although closer to estradiol than to progesterone. The reason is that the keto group of estrone in position 17 shows chemical properties slightly different to those of the keto group of progesterone in position 20. These keto groups transform in an enol function but in estrone originates a cycloalkane, which is much less favourable sterically than the linear alkene formed in progesterone. The enolate anion evolved in progesterone contributes to favouring its retention, thus increasing the capacity with pH.

On the other hand, DES is a nonsteroidal molecule, although with a behaviour similar to the steroids assayed. The reason is that DES structurally takes the form of estradiol and estrone with two open rings (B and C) and the D ring containing six-carbon atoms instead of five. Thus, the geometrical characteristics of DES, particularly the distance between the two OH groups, approximate those of estradiol and estrone, and consequently, their chromatographic behaviour.

4. Conclusion

The Gumbel distribution resulted in a powerful and robust approach to shape the asymmetric chromatographic peaks, behaving similarly or even better than the most widely accepted model in chromatography, the exponential modified Gaussian function. Further, we developed diverse equations to model the capacity factor by joining the simultaneous effect of several experimental variables and various quantum chemical parameters, achieving a good fit between the experimental and theoretical data. On the other hand, evaluation of the retention mechanism of the analytes was possible relating the chromatographic parameters with various structural features. The proposed retention mechanism for these compounds may be helpful to explain the retention mechanism of other drugs showing some structural and functional similarity but modulated by the size of the molecule and the aromatic system.

CRediT authorship contribution statement

F.J. Pereira: Methodology, Investigation. **R. López:** Formal analysis. **A. Rodríguez-Cordero:** Visualization. **L.C. Robles:** Visualization. **D. Suárez:** Formal analysis. **A.J. Aller:** Conceptualization, Writing -

review & editing.

Declaration of Competing Interest

The authors declare that they have no known competing financial interests or personal relationships that could have appeared to influence the work reported in this paper.

Acknowledgements

We produced molecular graphics images using the UCSF Chimera package from the Resource for Biocomputing, Visualization, and Informatics at the University of California, San Francisco (supported by NIH P41 RR-01081). The authors are also indebted to N. Díaz (University of Oviedo, Spain) to support quantum chemical calculations. We acknowledge support by the PGC2018-095953-B grant (MICINN, Spain), but this research did not receive any specific grant from funding agencies in the commercial or not-for-profit sectors.

Appendix A. Supplementary data

Supplementary data to this article can be found online at https://doi.org/10.1016/j.microc.2021.106693.

References

[1] I.G. Zenkevich, A.A. Makarov, A.A. Pavlovskii, New approaches to the calculation and interpretation of asymmetry factors of chromatographic peaks, J. Anal. Chem. 72 (7) (2017) 710–718, https://doi.org/10.1134/S1061934817070164.
[2] V.B. Di Marco, G.G. Bombi, Mathematical functions for the representation of chromatographic peaks, J. Chromatogr. A. 931 (1-2) (2001) 1–30, https://doi.org/10.1016/S0021-9673(01)01136-0.
[3] K. Miyabe, G. Guiochon, A kinetic study of mass transfer in Reversed-Phase Liquid Chromatography on a C18-silica gel, Biotechnol. Prog. Press. Anal. Chem. 72 (21) (2000) 5162–5171, https://doi.org/10.1021/ac0002801.
[4] J. Baeza-Baeza, M. García-Alvarez-Coque, Characterisation of chromatographic peaks using the linearly modified Gaussian model. Comparison with the bi-Gaussian and the Foley and Dorsey approaches, J. Chromatogr. A. 1515 (2017) 129–137, https://doi.org/10.1016/j.chroma.2017.07.087.
[5] K. Lan, J.W. Jorgenson, A hybrid of exponential and gaussian functions as a simple model of asymmetric chromatographic peaks, J. Chromatogr. A. 915 (1-2) (2001) 1–13, https://doi.org/10.1016/S0021-9673(01)00594-5.
[6] T.L. Pap, Z.s. Pápai, Application of a new mathematical function for describing chromatographic peaks, J. Chromatogr. A. 930 (1-2) (2001) 53–60, https://doi.org/10.1016/S0021-9673(01)01163-3.
[7] T. Yu, H. Peng, Quantification and deconvolution of asymmetric LC-MS peaks using the bi-Gaussian mixture model and statistical model selection, BMC Bioinf. 11 (1) (2010), https://doi.org/10.1186/1471-2105-11-559.
[8] A.F. Kadjo, P.K. Dasgupta, J. Su, S. Liu, K.G. Kraiczek, Width based quantitation of chromatographic peaks: principles and principal characteristics, Anal. Chem. 89 (7) (2017) 3884–3892, https://doi.org/10.1021/acs.analchem.6b04857.
[9] J. Li, Comparison of the capability of peak functions in describing real chromatographic peaks, J. Chromatogr. A. 952 (1-2) (2002) 63–70, https://doi.org/10.1016/S0021-9673(02)00090-0.
[10] M.F. Wahab, D.C. Patel, D.W. Armstrong, Total peak shape analysis: detection and quantitation of concurrent fronting, tailing, and their effect on asymmetry measurements, J. Chromatogr. A. 1509 (2017) 163–170, https://doi.org/10.1016/j.chroma.2017.06.031.
[11] A. Golubev, Exponentially modified peak functions in biomedical sciences and related disciplines, Comput. Math. Methods Med. 2017 (2017), https://doi.org/10.1155/2017/7925106.
[12] Y. Kalambet, Y. Kozmin, K. Mikhailova, I. Nagaev, P. Tikhonov, Reconstruction of chromatographic peaks using the exponentially modified Gaussian function, J. Chemom. 25 (2011) 352–356, https://doi.org/10.1002/cem.1343.
[13] N. Maljurić, B. Otašević, A. Malenović, M. Zečević, A. Protić, Quantitative structure retention relationship modeling as potential tool in chromatographic determination of stability constants and thermodynamic parameters of β-cyclodextrin complexation process, J. Chromatogr. A. 1619 (2020) 460971, https://doi.org/10.1016/j.chroma.2020.460971.
[14] L.R. Snyder, M.A. Quarry, J.L. Glajch, Solvent-strength selectivity in reversed-phase HPLC, Chromatographia 24 (1) (1987) 33–44, https://doi.org/10.1007/BF02688465.
[15] J. Dolan, L. Snyder, R. Wolcott, P. Haber, T. Baczek, R. Kaliszan, et al., Reversed-phase liquid chromatographic separation of complex samples by optimising temperature and gradient time: III. Improving the accuracy of computer, J. Chromatogr. A. 857 (1999) 41–68, https://doi.org/10.1016/S0021-9673(99)00766-9.
[16] K. Valkó, L.R. Snyder, J.L. Glajch, Retention in reversed-phase liquid chromatography as a function of mobile-phase composition, J. Chromatogr. A. 656 (1-2) (1993) 501–520, https://doi.org/10.1016/0021-9673(93)80816-Q.
[17] A. Andrés, M. Rosés, E. Bosch, Prediction of the chromatographic retention of acid–base compounds in pH buffered methanol–water mobile phases in gradient mode by a simplified model, J. Chromatogr. A. 1385 (2015) 42–48, https://doi.org/10.1016/j.chroma.2015.01.062.
[18] V.S. Joshi, V. Kumar, A.S. Rathore, Role of organic modifier and gradient shape in RP-HPLC separation: analysis of GCSF variants, J. Chromatogr. Sci. 53 (3) (2015) 417–423, https://doi.org/10.1093/chromsci/bmu222.
[19] S.N. Majumdar, A. Pal, G. Schehr, Extreme value statistics of correlated random variables: a pedagogical review, Phys. Rep. 840 (2020) 1–32, https://doi.org/10.1016/j.physrep.2019.10.005.
[20] S. Kotz, S. Nadarajah, Extreme value distributions: theory and applications, (2000).
[21] S. Purushothaman, S. Ayet San Andrés, J. Bergmann, T. Dickel, J. Ebert, H. Geissel, et al., Hyper-EMG: a new probability distribution function composed of Exponentially Modified Gaussian distributions to analyse asymmetric peak shapes in high-resolution time-of-flight mass spectrometry, Int. J. Mass Spectrom. 421 (2017) 245–254, https://doi.org/10.1016/j.ijms.2017.07.014.
[22] J.P. Foley, J.G. Dorsey, Equations for calculation of chromatographic figures of merit for ideal and skewed peaks, Anal. Chem. 55 (4) (1983) 730–737, https://doi.org/10.1021/ac00255a033.
[23] Joe P. Foley, Equations for chromatographic peak modeling and calculation of peak area, Anal. Chem. 59 (15) (1987) 1984–1987, https://doi.org/10.1021/ac00142a019.
[24] F.J. Pereira, A. Rodríguez-Cordero, R. López, L.C. Robles, A.J. Aller, Development and validation of an RP-HPLC-PDA method for determination of paracetamol, caffeine and tramadol hydrochloride in pharmaceutical formulations, Pharmaceuticals 14 (2021) 466, https://doi.org/10.3390/ph14050466.
[25] R. Core Team, A Language and Environment for Statistical Computing, R Found. Stat. Comput. (2020) https://www.R-project.org/.
[26] B Galabov, P Bobadova-Parvanova, S Ilieva, V Dimitrova, The electrostatic potential at atomic sites as a reactivity index in the hydrogen bond formation, J. Mol. Struct. THEOCHEM. 630 (1-3) (2003) 101–112, https://doi.org/10.1016/S0166-1280(03)00149-0.
[27] N.M. O'Boyle, M. Banck, C.A. James, C. Morley, T. Vandermeersch, G. R. Hutchison, Open Babel: an open chemical toolbox, J. Cheminformatics 3 (2011) 1–14, https://doi.org/10.1186/1758-2946-3-33.
[28] N. Sauton, D. Lagorce, B.O. Villoutreix, M.A. Miteva, MS-DOCK: accurate multiple conformation generator and rigid docking protocol for multi-step virtual ligand screening, BMC Bioinforma. 9 (2008) 1–12, https://doi.org/10.1186/1471-2105-9-184.
[29] A.D. Becke, Density-functional thermochemistry. III. The role of exact exchange, J. Chem. Phys. 98 (7) (1993) 5648–5652, https://doi.org/10.1063/1.464913.
[30] C. Lee, W. Yang, R.G. Parr, Development of the Colle-Salvetti correlation-energy formula into a functional of the electron density, Phys. Rev. B. 37 (2) (1988) 785–789, https://doi.org/10.1103/PhysRevB.37.785.
[31] T. Clark, J. Chandrasekhar, G.W. Spitznagel, P.V.R. Schleyer, Efficient diffuse function-augmented basis sets for anion calculations. III. The 3-21+G basis set for first-row elements, Li–F, J. Comput. Chem. 4 (1983) 294–301, https://doi.org/10.1002/JCC.540040303.
[32] P.C. Hariharan, J.A. Pople, The influence of polarisation functions on molecular orbital hydrogenation energies, Theor. Chim. Acta 28 (1973) 213–222, https://doi.org/10.1007/BF00533485.
[33] W.J. Hehre, R. Ditchfield, J.A. Pople, Self—consistent molecular orbital methods. XII. Further extensions of Gaussian—Type basis sets for use in molecular orbital studies of organic molecules, J. Chem. Phys. 56 (5) (1972) 2257–2261, https://doi.org/10.1063/1.1677527.
[34] A.V. Marenich, C.J. Cramer, D.G. Truhlar, Universal solvation model based on solute electron density and on a continuum model of the solvent defined by the bulk dielectric constant and atomic surface tensions, J. Phys. Chem. B. 113 (18) (2009) 6378–6396, https://doi.org/10.1021/jp810292n.
[35] S. Grimme, A. Hansen, J.G. Brandenburg, C. Bannwarth, Dispersion-corrected mean-field electronic structure methods, Chem. Rev. 116 (9) (2016) 5105–5154, https://doi.org/10.1021/acs.chemrev.5b00533.
[36] T.H. Dunning, Gaussian basis sets for use in correlated molecular calculations. I. The atoms boron through neon and hydrogen, J. Chem. Phys. 90 (2) (1989) 1007–1023, https://doi.org/10.1063/1.456153.
[37] D.E. Woon, T.H. Dunning, Gaussian basis sets for use in correlated molecular calculations. V. Core-valence basis sets for boron through neon, J. Chem. Phys. 103 (11) (1995) 4572–4585, https://doi.org/10.1063/1.470645.
[38] M.J. Frisch, G.W. Trucks, H.B. Schlegel, G.E. Scuseria, M.A. Robb, J.R. Cheeseman, et al., Gaussian 16, Revision C.01, Wallingford CT, 2016.
[39] D. Hait, M. Head-Gordon, How accurate is density functional theory at predicting dipole moments? An assessment using a new database of 200 benchmark values, J. Chem. Theory Comput. 14 (4) (2018) 1969–1981, https://doi.org/10.1021/acs.jctc.7b01252.
[40] D. Hait, M. Head-Gordon, How accurate are static polarizability predictions from density functional theory? An assessment over 132 species at equilibrium geometry, Phys. Chem. Chem. Phys. 20 (30) (2018) 19800–19810, https://doi.org/10.1039/C8CP03569E.
[41] L. Goerigk, S. Grimme, A general database for main group thermochemistry, kinetics, and noncovalent interactions - assessment of common and reparameterised (meta-)GGA density functionals, J. Chem. Theory Comput. 6 (2010) 107–126, https://doi.org/10.1021/ct900489g.

[42] A.D. Becke, Density-functional thermochemistry. IV. A new dynamical correlation functional and implications for exact-exchange mixing, J. Chem. Phys. 104 (3) (1996) 1040–1046, https://doi.org/10.1063/1.470829.
[43] F. Neese, The ORCA program system, WIREs Comput. Mol. Sci. 2 (1) (2012) 73–78.
[44] F. Neese, Software update: the ORCA program system, version 4.0, Wiley Interdiscip, Rev. Comput. Mol. Sci. 8 (1) (2018), https://doi.org/10.1002/wcms.1327.
[45] E.F. Pettersen, T.D. Goddard, C.C. Huang, G.S. Couch, D.M. Greenblatt, E.C. Meng, et al., UCSF Chimera - a visualisation system for exploratory research and analysis, J. Comput. Chem. 25 (2004) 1605–1612, https://doi.org/10.1002/jcc.20084.
[46] M.F. Sanner, A.J. Olson, J. Spehner, Reduced surface: an efficient way to compute molecular surfaces, Biopolymers 38 (1996) 305–320, https://doi.org/10.1002/(SICI)1097-0282(199603)38:3<305::AID-BIP4>3.0.CO;2-Y.
[47] ICH, International conference on harmonisation of technical requirements for registration of pharmaceuticals for human use. ich harmonised tripartite guideline. validation of analytical procedures: text and methodology Q2(R1), Geneva, Switzerland, 2005.
[48] N.M. Putintsev, N.V. Dolgopyatova, D.N. Putintsev, Calculating the permittivity and polarizability of methanol–water mixtures at 20°C, Russ. J. Phys. Chem. A 90 (10) (2016) 2101–2103, https://doi.org/10.1134/S0036024416100216.
[49] P. Wang, A. Anderko, Computation of dielectric constants of solvent mixtures and electrolyte solutions, Fluid Phase Equilib. 186 (1-2) (2001) 103–122, https://doi.org/10.1016/S0378-3812(01)00507-6.
[50] K.S. Kanse, S.D. Chavan, C.S. Mali, A.C. Kumbharkhane, S.C. Mchrotra, Structural study of methanol-water mixture from dielectric parameters, Indian J. Phys. 80 (2006) 265–269.
[51] G. Gilli, P. Gilli, Towards an unified hydrogen-bond theory, J. Mol. Struct. 552 (1-3) (2000) 1–15, https://doi.org/10.1016/S0022-2860(00)00454-3.
[52] B.K. Paul, N. Guchhait, Geometrical criteria versus quantum chemical criteria for assessment of intramolecular hydrogen bond (IMHB) interaction: a computational comparison into the effect of chlorine substitution on IMHB of salicylic acid in its lowest energy ground state conformer, Chem. Phys. 412 (2013) 58–67, https://doi.org/10.1016/J.CHEMPHYS.2012.12.006.
[53] https://www.ncbi.nlm.nih.gov., 2020.
[54] A. Pagliara, B. Testa, P.-A. Carrupt, P. Jolliet, C. Morin, D. Morin, et al., Molecular properties and pharmacokinetic behavior of Cetirizine, a Zwitterionic H1-receptor antagonist, J. Med. Chem. 41 (6) (1998) 853–863, https://doi.org/10.1021/jm9704311.